A stochastic modelling for LES of a two-phase combusting flow

W.P. Jones, A.J. Marquis, D. Noh*

Department of Mechanical Engineering, Imperial College London, London, UK

Abstract

This current investigation attempts to conduct Large Eddy Simulation (LES) of a turbulent particle-laden combusting experiment where methanol liquid fuel is injected using a Research Simplex Atomizer (RSA), i.e. a type of pressure-swirl atomizers. The quality of the computational grid and the set-up of inlet/boundary conditions are validated by simulating an isothermal test case. However, non-reacting and reacting cases with a stochastic breakup model are to be carried out in the future as the reproduction of spray properties using Rosin-Rammler distribution was found to be poor.

Introduction

There are numerous engineering applications in industry such as diesel engines, gas turbines and rocket engines where liquid fuels are often delivered into combustion chambers via a means of the atomization. When a column of liquid fuels is discharged into a gas flow, it becomes unstable and disintegrates into smaller droplets which then evaporate, create fuel vapour mixing with the surrounding gas and burn. This atomization process plays a key role in determining the overall performance of two-phase combustion flows in terms of the rate of fuel consumption and pollutant emissions. The design of spray injection systems leading to a reduction in the final size of atomized droplets and hence an increase in fuel evaporation rates is also vital because improvements in the combustion efficiency can be achieved. Consequently, researchers have made many attempts to numerically investigate the challenging issues in chemically reacting flows with spray fuels. Historically, the atomization process has been calculated by the widely accepted breakup models such as Taylor analogy breakup (known as TAB) [1] and the wave model by Reitz and Diwakar [2]. The TAB breakup model is based upon Taylor's analogy to represent the oscillation of mother droplets as a spring-mass system while the wave model used a linear stability analysis of liquid jets to determine the unstable growth of Kelvin-Helmholtz waves on the surface of the injected liquid 'blobs'.

In the context of Large Eddy Simulation (LES), the deterministic breakup models have not gained popularity as they are suitable mainly to RANS computations. There have not been many attempts which investigate the atomization of droplets using LES calculations but Apte et al. [3] are among a few which developed a stochastic *sgs* model for LES of atomizing spray. The model is based on Kolmogorov's discrete model which is rewritten in the form of Fokker-Planck equation to formulate the probability of size of daughter droplets. A stochastic model for the spray atomization developed by Jones and Lettieri [4] is adopted in the present work. A Monte Carlo trajectory integration is used to reproduce the influence of gas phase fluctuating motions on the secondary breakup of droplets. The adopted breakup model has been validated with the experiment of Park et al. [5] and the measurement of Hiroyasu and Kadota [6].

In this paper, the LES code known as BOFFIN-LES [7], i.e. in-house, block-structured, parallel, incompressible with variable density code, is applied to investigate the complex phenomena such as turbulence-chemistry interaction and atomization of liquid fuel in an academic burner with a turbulent methanol/air spray flame [8,9]. To the authors' knowledge, this present work appears to be a first attempt to simulate the breakup of droplets from the injection point. There have been several previous attempts [10,11] but measurements were used to define inlet conditions such as the gas velocity statistics and spray properties in their computations rather than here where we have used the physical geometry.

The structure of the paper is constructed as follows. Firstly, the mathematical modelling including the filtered LES equations and the stochastic models for droplet dispersion, evaporation and breakup is explained. A brief description of the experimental configuration under consideration and the inlet/boundary conditions applied is then presented. All the statistics are compared between experimental measurements and predictions from LES calculations. Finally, the conclusions of the present work are made.

Mathematical models

LES equations: interaction of gas and liquid phase

In LES calculations, a low-pass, density-weighted filter is applied to the conservation equations of mass, momentum and scalars such as enthalpy and species mass fraction. As a result, a separation of the unresolved *sgs* from the large scale energy-containing motions can be obtained. The large energetic motions are then computed directly while the effects of the *sgs* motions on the resolved flow field are accounted for by a means of modelling. The density-weighted filtered governing equations of the low-Mach number, variable density flow with the influence of the dispersed phase can be expressed as:

$$\frac{\partial \bar{\rho}}{\partial t} + \frac{\partial \bar{\rho} \tilde{u}_i}{\partial x_i} = \overline{\dot{S}}_m \qquad (1)$$

*Corresponding author: dongwon.noh10@imperial.ac.uk

$$\frac{\partial \bar{\rho}\tilde{u}_i}{\partial t}+\frac{\partial \bar{\rho}\tilde{u}_i\tilde{u}_j}{\partial x_j}=-\frac{\partial \bar{p}}{\partial x_i}+\frac{\partial \bar{\sigma}_{ij}}{\partial x_j}+\frac{\partial \tau_{ij}^{sgs}}{\partial x_j}+\overline{\dot{S}}_{mom,i} \quad (2)$$

$$\frac{\partial \bar{\rho}\tilde{\phi}_\alpha}{\partial t}+\frac{\partial \bar{\rho}\tilde{\phi}_\alpha\tilde{u}_j}{\partial x_j}=\frac{\partial}{\partial x_j}\left(\frac{\mu}{\sigma}\frac{\partial \tilde{\phi}_\alpha}{\partial x_j}\right)-\frac{\partial J_k}{\partial x_j} +\overline{\rho\dot{\omega}(\underline{\phi})}+\overline{\dot{S}}_\alpha \quad (3)$$

where ρ, u_i, p and ϕ_α (Y_α or h) represent the fluid density, velocity in i-th direction, pressure and relevant scalars such as mass fraction of species α or enthalpy h respectively. The unknown *sgs* stresses τ_{ij}^{sgs} appearing in the filtered momentum equation are dealt with via a dynamic version of the Smagorinsky model [12]. For the species and enthalpy equations, a Lewis number of unity is assumed so that σ is the Schmidt or Prandtl number as required. Equation (3) includes the unclosed *sgs* flux J_k and filtered chemical source term $\overline{\rho\dot{\omega}(\underline{\phi})}$. The chemical source term which represents the net formation rate of species α due to chemical reactions necessitates an appropriate modelling because of a high degree of its nonlinearity. The model adopted in the current work is the Eulerian stochastic field method which is based on a transported *pdf* approach (see [13] for more detail).

The phase exchange source terms can be obtained from a summation of the effects of every p-th particle instantaneously located in a specific filter volume Δ, e.g. $\bar{\dot{S}}_m = -\frac{1}{\Delta^3}\sum_{p=1}^{N_p}\dot{m}_p$. The momentum exchange between the continuous and the dispersed phase is achieved through $\bar{\dot{S}}_{mom,i}$ in order to take into account the gas phase turbulence modulation by the presence of spray. Furthermore, the evaporation of drops will contribute to sources of mass and Y_α for the gas phase via $\bar{\dot{S}}_m$ and $\bar{\dot{S}}_{Y_\alpha}$ respectively while the exchange of source of enthalpy $\dot{S}_h$ occurs when the heating and cooling of drops take place as a result of the heat transfer between the gas and liquid phases and evaporation of the droplets.

Modelling of droplet dispersion and acceleration

A stochastic Markov model based on the work of Bini and Jones [14,15] is adopted to characterise the influence of the *sgs* motions on the dispersion of droplets. The change of the *p*-th droplet velocity over a time dt can be expressed as:

$$d\boldsymbol{u}_p=\frac{\bar{\boldsymbol{u}}-\boldsymbol{u}_p}{\tau_p}dt+\left(C_o\frac{k_{sgs}}{\tau_t}\right)^{1/2}d\boldsymbol{W}_t +\left(1-\frac{\rho_g}{\rho_l}\right)\boldsymbol{g}dt \quad (4)$$

where $\bar{\boldsymbol{u}}$ and ρ_g represent the filtered gas velocity and density interpolated at the location of individual droplet, ρ_l are the droplet density, $\boldsymbol{g}$ is the gravitational acceleration and $\tau_p^{-1}=\frac{3}{4}\frac{\rho_g C_D}{\rho_l D_p}|\bar{\boldsymbol{U}}_s|$ denotes the particle relaxation time. D_p is the particle diameter and $|\bar{\boldsymbol{U}}_s|$ is the slip velocity. The drag coefficient C_D which is a function of Reynolds number is calculated from the drag law formulated by Yuen and Chen [16]. The stochastic term consists of a model constant C_o taken as unity and the *sgs* kinetic energy k_{sgs} which accounts for the effects of the *sgs* stresses on the particle dispersion via the use of the Wiener process $d\boldsymbol{W}_t$. The interaction between droplets and gas phase turbulence is taken into account by the following time scale:

$$\tau_t=\frac{\tau_p^{1.6}}{\left(\Delta/k_{sgs}^{1/2}\right)^{0.6}} \quad (5)$$

The *sgs* time scale with α = 0.8 was able to reproduce a highly-tailed *pdf* of particle accelerations observed experimentally [14].

Abramzon and Sirignano [17] reviewed the classical droplet evaporation model and further developed in order to include the effect of the Stefan flow on heat and mass transfer between droplets and the surrounding gas. The Abramzon-Sirignano model is adopted in the present work to characterise the instantaneous droplet evaporation rate from the following equations:

$$dT_p=-\frac{\dot{m}_p}{m_p B_T'}\left(\frac{C_{p,g}}{C_{p,l}}\right)(\bar{T}_g-T_p)dt +\left(\frac{h_{fg}}{C_{p,l}}\right)\frac{\dot{m}_p}{m_p}dt \quad (6)$$

$$dm_p=-\frac{m_p}{3Sc_g\tau_p}(Sh^{dt}+Sh^{sgs})ln(1+B_M)dt \quad (7)$$

where T_p and $\bar{T}_g$ represent the droplet temperature and the filtered gas phase temperature, $C_{p,l}$ and $C_{p,g}$ are the liquid and gas specific heat capacities, h_{fg} is the latent heat of vaporisation and B_M and $B_T^{'}$ are the Spalding mass and heat transfer numbers respectively. The Nusselt and Sherwood numbers, Nu and Sh, are calculated using the method of Clift et al. [18]. Like a classical decomposition of velocity components, the Sherwood number is decomposed into the resolved contribution Sh^{dt} and the unresolved part Sh^{sgs} in order to account for the influence of unknown *sgs* fluctuations on the evolution of droplet mass:

$$Sh^{sgs}dt=C_v Sc_g^{1/3}\left(\rho_g\frac{k_{sgs}^{1/2}D_p}{\mu_g}\right)^{1/2}|d\boldsymbol{W}_t|^{1/2}\tau_p^{3/4} \quad (8)$$

where $d\boldsymbol{W}_t$ is the increment of the Wiener process and C_v is a model constant taken as 1.0 [19].

Droplet secondary breakup

The current breakup model consists of a deterministic contribution mainly due to aerodynamic forces imposed on droplets by the surrounding gas and a stochastic formulation which is a function of both the droplet diameter and the dissipation rate of turbulent kinetic energy:

$$f_{bu} = \frac{1}{\pi}\sqrt{\frac{8\sigma}{\rho_l r_0^3}} + K_g \frac{\sqrt{\beta\left(2\epsilon r_0\right)^{2/3} - 12\sigma/(2\rho r_0)}}{2r_0} \quad (9)$$

where f_{bu} is the breakup frequency, σ is the surface tension of liquid, r_0 is the radius of mother droplet and ϵ is the dissipation rate of turbulent kinetic energy. The first term in Eq. 9 is the deterministic contribution of the secondary breakup frequency determined when droplets experience fragmentation in the bag breakup regime, i.e. $12 \leq We \leq 50$ [20]. The typical Weber number of droplets in the experimental burner under consideration is well within the bag breakup regime. For large Weber number, the breakup frequency is given by $f_{det} = C_{bu}\sqrt{\frac{\rho_g}{\rho_l}}\frac{r_0}{|\widetilde{U}_s|}$ where $C_{bu} = \sqrt{1/3}$ [1].

According to Martínez-Bazán et al. [21,22] who experimentally investigated the breakup of air bubbles in a turbulent air flow, the stochastic component of the breakup frequency contains the rate of dissipation of kinetic energy which requires a reliable knowledge. In the context of LES, it can be obtained from $\epsilon = 2\left(v + v_{sgs}\right)\tilde{S}_{ij}\tilde{S}_{ij}$ where $\tilde{S}_{ij}$ is the filtered strain tensor. Although the empirical constants being K_g = 0.25 and β = 8.2 were determined by considering the breakup of air bubbles immersed in a water jet, they are retained in the current work. Applying the fragmentation model of Martínez-Bazán et al. to the present case is possible because it was adopted by Lasheras and Hopfinger [23] in order to study the far-field breakup of a liquid jet by a high speed annular gas jet.

Martínez-Bazán et al. also proposed a statistical model to determine the probability density function of the size of daughter particles resulting from the breakup of a mother particle. The model assumes a mechanism of binary droplet breakup leading to daughter droplet diameters D_1 and $D_2 = D_0\left[1 - \left(D_1/D_0\right)^3\right]^{1/3}$ when a mother droplet with its size of D_0 breaks. However, Martínez-Bazán and others [24] reviewed the model for the daughter size *pdf* and suggested the corrected version which satisfies the volume-conserving condition as follows:

$$f^*\left(D^*\right) = \frac{D^{*2}\left[D^{*2/3} - \Lambda^{5/3}\right]\left[\left(1 - D^{*3}\right)^{2/9} - \Lambda^{5/3}\right]}{\int_{D^*_{min}}^{D^*_{max}} D^{*2}\left[D^{*2/3} - \Lambda^{5/3}\right]\left[\left(1 - D^{*3}\right)^{2/9} - \Lambda^{5/3}\right] dD^*} \quad (10)$$

where $D^* = D_1/D_0$ and $\Lambda = D_c/D_0$. The critical diameter, $D_c = \left[12\sigma/(\beta\rho)\right]^{3/5}\epsilon^{-2/5}$, simply represents the diameter of the largest droplet which will not undergo any fragmentation under the turbulent action of the flow.

Test case configuration

Experimental burner

The experimental configuration under consideration was designed by McDonell et al. [25] at the University of California, Irvine Combustion Laboratory. A dilute methanol spray is injected using the Research Simplex Atomizer (RSA) alongside an air passage through which three different modes such as simplex (no atomizing air), non-swirling air-assist and swirling air-assist are operated. In the present work, the second operating mode will only be studied. The simplex tip delivers liquid fuel at a spray angle of 85 degrees in full. The injection assembly with a hole of 4.9 mm in diameter is mounted at a 495 $\times$ 495 square duct. In the combustion chamber, there is an additional air passage coflowing with the atomizer flows at an average velocity of 1.0 m/s. The experiment was carried out at atmospheric pressure and room temperatures between 18 and 25 °C. A mass flow rate of air is 1.32 g/s resulting in a pressure drop of 3.73 kPa while the liquid fuel is injected at 1.26 g/s corresponding to Δp_l = 420 kPa.

In the experimental work, the axial and radial components of gas, mean concentration of methanol vapour, gas temperature, liquid flux, droplet velocities as a function of size class and droplet size distributions were measured at several axial locations: 7.5, 15, 50, 75, 100 and 150 mm away from the nozzle exit. Detailed comparisons will be made at the following four locations, i.e. 15, 50, 75 and 100 mm unless otherwise stated. The gas and droplet velocity components and droplet size were obtained using phase Doppler interferometry (PDI) while infrared extinction/scattering (IRES) was adopted to measure the vapour concentration.

Computational set-up

BOFFIN-LES is used for simulations presented in this paper. An isothermal test case was initially conducted in order to validate the quality of the grid applied to the computational domain. Figure 1 represents a detailed description of the computational mesh in the vicinity of the liquid fuel injection. A structured, multi-block mesh of the considered burner was produced using ICEM CFD and includes 1.4 million cells and 162 blocks. The computational domain extending 30D radially and 100D axially is composed of the nozzle in which the liquid fuel is injected and main combustion chamber. A local refinement in the size of the computational grid is made in the region near the nozzle exit where the breakup of methanol droplets, mixing of fuel vapour and air and shear layer of the expanding air jet take place. A zero gradient boundary condition was experimentally observed at roughly 180 mm away from the centreline but free slip conditions are applied along the outer plane of the computational domain located at 150 mm away from the centreline. This is justified because of the presence of the zero gradient in all the measured quantities well before the symmetry plane experimentally measured. Furthermore, the exit plane of the domain is assigned with non-reflecting outflow boundary conditions.

A non-reactive case with methanol spray was carried out by assuming the possible distribution of the size of droplets being injected and using the stochastic breakup model. As discussed later on, it is in progress in order to correctly reproduce spray characteristics such as the droplet number density and Sauter mean diameter (SMD

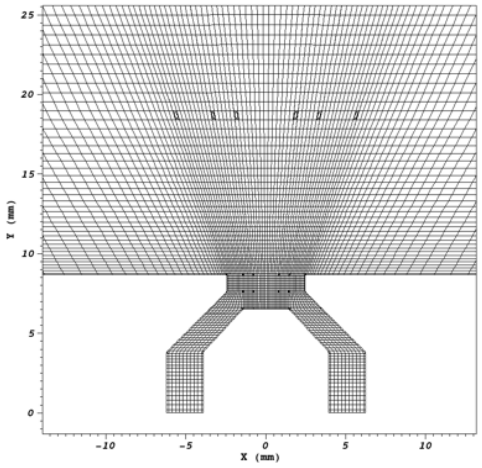

Figure 1: A detailed view of grid close to the injector

or D_{32}) and the concentration of fuel vapour. When the reactive test case is under investigation, a reduced reaction mechanism with 14 reaction steps and 18 chemical species [26] will be used to represent the gas phase reaction of methanol/air spray flame. The interaction of gas-phase *sgs* turbulence and chemistry will be described by adopting the stochastic fields/*sgs pdf* equation method with 8 stochastic fields.

The gas temperature and pressure were set to be 293.15 K and 1 atm throughout the computational domain and the inlet plane. In order to represent a spatially and temporally inhomogeneous inlet flow through the main inlet, digital turbulent inflow conditions first proposed by Klein et al. [27] were used and the resulting accuracy was assured by checking the mean axial velocity at the nozzle exit, i.e. 62.5 m/s measured from the experiment [25]. The experimental measurement for the coflow at the axial location of 7.5 mm was used to assign the axial velocity component of the air through the coflow. In the case of the non-reacting flow with the presumed droplet size distribution, the Rosin-Rammler distribution law [28] with the mean size of around 35.0 μm and a constant of 3.6 determining the spread of droplet sizes was adopted. There are several empirical correlations to determine the velocity of the injected liquid sheet and its initial sheet thickness forming at the exit of the injector (More detail can be found in [28]). This requires a knowledge of the injected liquid mass flow rate, the spray angle, the diameter of the injector and liquid properties which are all given from the experimental database. The spray velocity and initial film thickness were calculated to be 22.8 m/s and 95 μm respectively. In the non-reacting case with the use of the breakup model, droplets with a diameter equal to the calculated sheet thickness are injected at the centre of the injection plane, satisfying the measured mass flow rate of liquid.

Results and discussion

Isothermal case

The isothermal test case was carried out with a time step of around 0.4 μs. A flow-through time based on the bulk velocity at the nozzle exit and the length of the computational domain, i.e. 0.5 m, is 0.008 s corresponding to 20,000 time steps. In order to flush initial disturbances induced by inlet conditions out of the computational domain, 10 flow-through times were initially performed. Another 30 flow-through times were simulated in order to present all the statistical results for the isothermal case.

The measured gas velocity statistics are compared with those predicted from the LES simulation at the four axial locations, i.e. 15, 50, 75 and 100 mm, as represented in Figs. 2 and 3. Radial profiles of the mean and fluctuating axial velocities reveal that the spreading rate of the air jet, the peak value of the velocity component along the centreline and the turbulence intensity are reproduced with the high level of accuracy. The use of the digital turbulence generator at the main inlet and the quality of the computational mesh are therefore demonstrated.

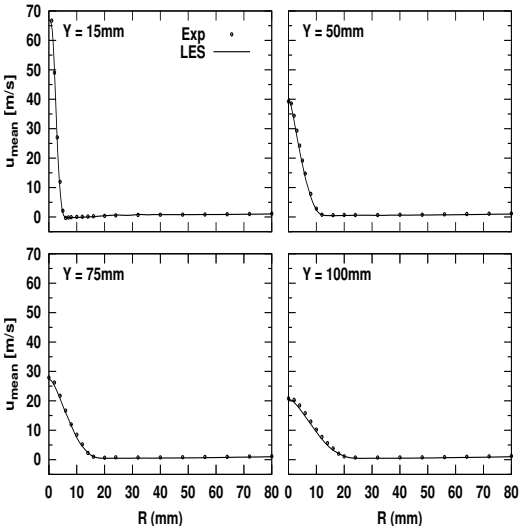

Figure 2: Radial profiles of mean axial velocities

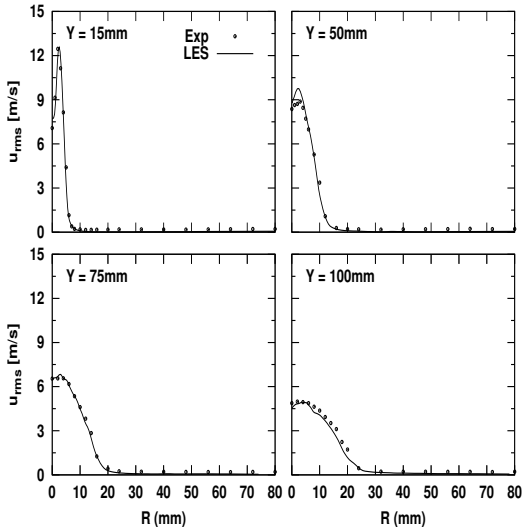

Figure 3: Radial profiles of fluctuating axial velocities

Non-reactive case

The non-reactive cases with the Rosin-Rammler ex-

pression were initiated with solutions from the isothermal case at 200,000 time steps in order to avoid the presence of the initial disturbances. Statistics shown here were collected over further 300,000 time steps corresponding to 15 flow-through times.

Figure 4 represents the instantaneous velocity field with a snapshot of individual droplets to provide a general impression on how they are dispersed in the gas. In general, droplets within small size classes tend to quickly travel towards the centreline as they almost immediately lose their initial momentum once discharged from the liquid injection point. On the other hand, those with a larger diameter are more likely to resist the momentum transfer from the surrounding gas and hence retain the injected spray angle for a longer distance.

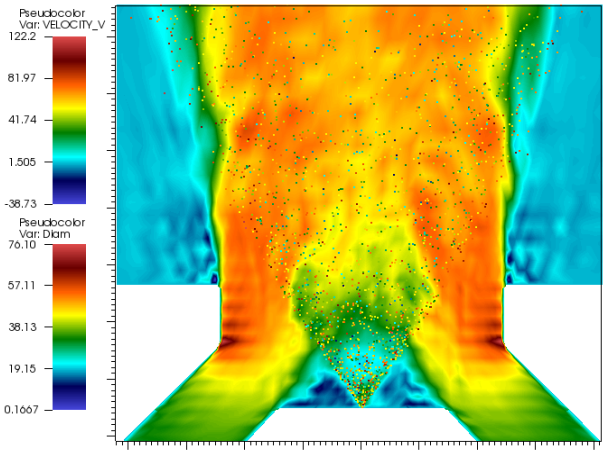

Figure 4: A contour plot of the velocity field with droplet motions in the region close to the injection plane

The measured and simulated SMD are compared in fig. 5. A relatively good agreement is achieved along the radial direction at the first two measurement locations while the mean diameter of droplets from the simulation then tends to diverge from the experimental data in the region near the centreline.

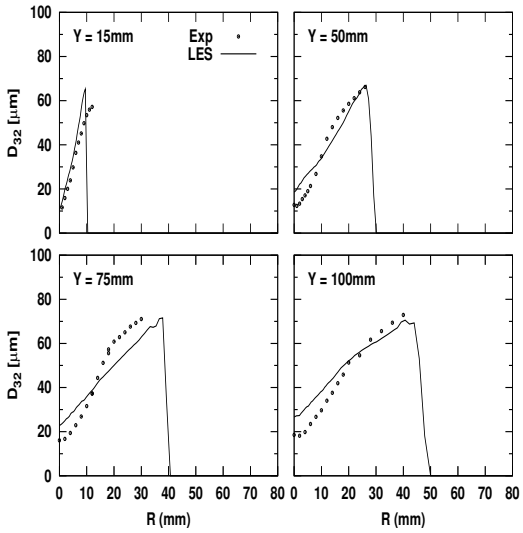

Figure 5: Radial profiles of Sauter Mean Diameter

A comparison of the droplet number density makes it more obvious that the presumed droplet size distribution does not result in a good reproduction of the droplet dispersion. As discussed before, the smallest droplets are easily convected by the gas flow towards the centreline. As a result, the predicted number density at the centreline does not increase along the axial distance because most of the droplets with small sizes may well move to the centreline well before the first measurement location. On the other hand, the measured number density at the centreline keeps increasing along the axial distance as larger droplets undergo fragmentations into smaller droplets which then travel towards the centreline and increase the local number density.

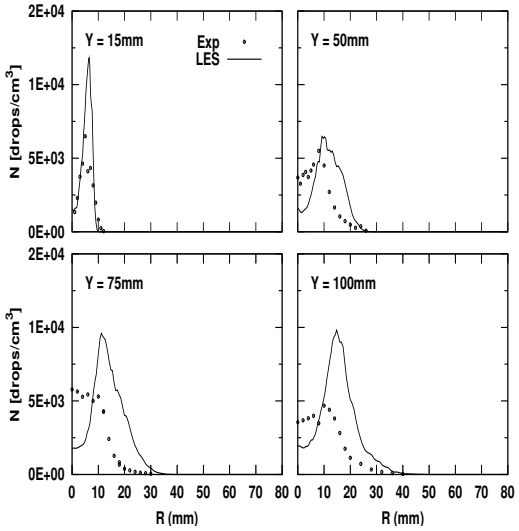

Figure 6: Radial profiles of droplet number density

Next, the concentration of methanol fuel vapour is compared in fig. 7 at four axial locations but slightly different from the previous comparisons, i.e. the first measurement location from 15 mm to 7 mm. The concentration is overestimated away from the centreline because of the presence of large droplets in the simulation which evaporate and increase the mass fraction of the fuel vapour. The results discussed so far have led to a strong necessity of using the stochastic breakup model in order to properly simulate the fundamental mechanisms of atomization. Unfortunately, the non-reacting case with the breakup model has not been completed so no comparisons can be made in the paper.

Conclusions

To date, a good agreement has been achieved only for the isothermal test case without the presence of methanol droplets. The excellent reproduction of the gas phase velocity statistics confirms the quality of the computational grid and the inlet/boundary conditions applied. However, further work is required as the predicted spray characteristics differ substantially from the measurements. In the foreseen future, the non-reacting and reacting cases will be conducted with the aid of the stochastic breakup model and its validity will be made over the considered

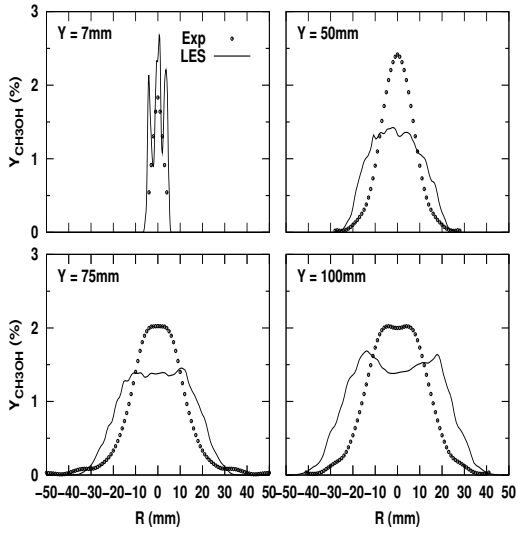

Figure 7: Radial profiles of methanol fuel vapour concentration

experimental configuration.

Acknowledgements

The present work received supports from the 7th Framework Programme of the European Union (FP7/2007-2013) under the Grant Agreement ACP0-GA-2011-265586.

References

[1] P.J. O'Rourke, A.A. Amsden, SAE Technical Paper (1987) 872089.
[2] R. Reitz, R. Diwakar, SAE Technical Paper (1987) 870598.
[3] S.V. Apte, M. Gorokhovski, P. Moin, Int. J. Multiphase Flow 29 (2003) 1503-1522.
[4] W.P. Jones, C. Lettieri, Phys. Fluids 22 (2010) 1-12.
[5] S.W. Park, S. Kim, C.S. Lee, Int. J. Multiphase Flow 32 (2006) 807-822.
[6] H. Hiroyasu, T. Kadota, SAE Technical Paper (1974) 74071.
[7] W.P. Jones, F. di Mare, A.J. Marquis, LES-BOFFIN: User's Guide, 2002.
[8] V.G. McDonell, M. Adachi, G.S. Samuelsen, Atomization Sprays 3 (1993) 389-410.
[9] V.G. McDonell, M. Adachi, G.S. Samuelsen, Atomization Sprays 3 (1993) 411-436.
[10] H.-W. Ge, E. Gutheil, Combust. Flame 153 (2008) 173-185.
[11] H.-W. Ge, E. Gutheil, Atomization Sprays 16 (2006) 531-542.
[12] U. Piomelli, Prog. Aero, Sci. 35 (1999) 335-362.
[13] L. Valino, Flow. Turbul. Combust. 60 (1998) 157-172.
[14] M. Bini, W.P. Jones, Phys. Fluids 19 (3) (2007) 035104.
[15] M. Bini, W.P. Jones, J. Fluid Mech. 614 (2008) 207.
[16] M.C. Yuen, L.W. Chen, Combust. Sci. Technol. 14 (4-6) (1976) 147-154.
[17] B. Abramzon, W.A. Sirignano, Int. J. Heat Mass Transfer 32 (9) (1989) 1605-1618.
[18] R. Clift, J.R. Grace, M.E. Weber, *Bubbles, Drops and Particles*, Academic Press, New York, 1978.
[19] M. Bini, W.P. Jones, Int. J. Heat Fluid Flow 30 (2009) 471-480.
[20] M. Pilch, C.A. Erdman, Int. J. Multiphase Flow 13 (6) (1987) 741-757.
[21] C. Martínez-Bazán, J.L. Montañés, J.C. Lasheras, J. Fluid Mech. 401 (1999) 157-182.
[22] C. Martínez-Bazán, J.L. Montañés, J.C. Lasheras, J. Fluid Mech. 401 (1999) 183-207.
[23] J.C. Lasheras, E.J. Hopfinger, Annu. Rev. Fluid Mech. 32 (2000) 275-308.
[24] C. Martínez-Bazán, J. R-Rodríguez, G.B. Deane, J.L. Montañés, J.C. Lasheras, J. Fluid Mech. 661 (2010) 159-177.
[25] V.G. McDonell, G.S. Samuelsen, J. Fluids Eng. 177 (1995) 145-153.
[26] R.P. Lindstedt, M.P. Meter, Proc. Combust. Inst. 29 (2002) 1395-1402.
[27] M. Klein, A. Sadiki, J. Janicka, J. Comput. Phys. 186 (2003) 652-665.
[28] A.H. Lefebvre, *Atomization and Sprays*, CRC press, 1988.